Fusion of ^{40}Ca + ^{40}Ca and other Ca + Ca systems near and below the barrier

G. Montagnoli,[1] A. M. Stefanini,[2] C. L. Jiang,[3] H. Esbensen,[3] L. Corradi,[2] S. Courtin,[4] E. Fioretto,[2] A. Goasduff,[4] F. Haas,[4] A. F. Kifle,[2] C. Michelagnoli,[1] D. Montanari,[1] T. Mijatović,[5] K. E. Rehm,[3] R. Silvestri,[2] Pushpendra P. Singh,[2] F. Scarlassara,[1] S. Szilner,[5] X. D. Tang,[6] and C. A. Ur[1]

[1]*Dipartimento di Fisica, Università di Padova, and INFN, Sezione di Padova, IT-35131 Padova, Italy*

[2]*INFN, Laboratori Nazionali di Legnaro, IT-35020 Legnaro (Padova), Italy*

[3]*Physics Division, Argonne National Laboratory, Argonne, Illinois 60439, USA*

[4]*IPHC, CNRS-IN2P3, Université de Strasbourg, FR-67037 Strasbourg Cedex 2, France*

[5]*Ruđer Bošković Institute, HR-10002 Zagreb, Croatia*

[6]*University of Notre Dame, Notre Dame, Indiana 46556, USA*

(Received 28 October 2011; revised manuscript received 4 January 2012; published 10 February 2012)

The fusion excitation function of ^{40}Ca + ^{40}Ca has been measured from well above the Coulomb barrier, down to low energies where the cross section is as small as $\simeq$20 μb, and the astrophysical S factor possibly reaches a maximum vs energy. The results of coupled-channels calculations using the M3Y + repulsion potential are presented. A detailed comparison is made with recently published data on the fusion of ^{40}Ca + ^{48}Ca and of ^{48}Ca + ^{48}Ca, including the excitation functions, their low-energy slopes and the barrier distributions. The presence of the fusion hindrance phenomenon in all cases is pointed out, as well as the influence of the strong octupole excitation in ^{40}Ca and of nucleon transfer channels with positive Q values in ^{40}Ca + ^{48}Ca.

DOI: 10.1103/PhysRevC.85.024607 PACS number(s): 25.70.Jj, 24.10.Eq

I. INTRODUCTION

Heavy-ion fusion reactions are dramatic events implying the rearrangement of all nucleons on new nuclear orbitals; however, cross sections near and below the Coulomb barrier are determined, to a large extent, by low-energy surface modes of the two interacting nuclei. The interest in studying fusion of various combinations of calcium isotopes dates back to the early 1980s [1], when the newly discovered phenomenon of sub-barrier "fusion enhancement" prompted various groups to study different behaviors in several mass regions [2]. The closed-shell structure of ^{40}Ca and ^{48}Ca immediately attracted the interest of both experimentalists and theoreticians [3]. Fusion of ^{40,48}Ca + ^{48}Ca was investigated again later on [4] with the goal of extracting fusion barrier distributions from accurate measurements of the excitation functions [5,6]. Detailed effects of the octupole phonons of both calcium isotopes were suggested by N. Rowley in a more recent study [7].

A renewed interest has developed in the last few years in the context of what is commonly known as the fusion hindrance phenomenon which occurs at far sub-barrier energies [8–10]. Fusion hindrance is generally associated with a steep slope of the excitation function well below the Coulomb barrier, when standard coupled-channels (CC) calculations are taken as reference. In this sense, medium-light systems such as ^{48}Ca + ^{48}Ca [11] do show hindrance, even if the logarithmic slopes saturate below the value expected for a constant astrophysical S factor [12],

$$L_{CS}(E) = \frac{\pi\eta}{E},$$

where $\eta = Z_1 Z_2 e^2/(\hbar v)$ is the Sommerfeld parameter. Consequently, the S factor does not have a maximum in the measured energy range.

The fusion of ^{40}Ca + ^{48}Ca was studied very recently [13]. The fusion excitation function has been extended downward by two orders of magnitude with respect to previous data [1,4], showing a steep slope at low energies, reaching the $L_{CS}(E)$ value. On the basis of this, a correlation between fusion hindrance and neutron excess $N - Z$ has been suggested [13].

Therefore, we decided to measure fusion cross sections for ^{40}Ca + ^{40}Ca, 16 neutrons less than ^{48}Ca + ^{48}Ca, in the whole relevant energy range. The data by Aljuwair *et al.* [1] extend only down to about 200 μb and with rather large experimental errors. The corresponding logarithmic derivative (slope) rises toward the L_{CS} value, but extrapolating to lower energies is rather uncertain. This excitation function is definitely inadequate to characterize the fusion cross section trend at deep sub-barrier energies. In this article, we present the results of the experiment on ^{40}Ca + ^{40}Ca, and we point out similarities and differences when comparing with ^{40}Ca + ^{48}Ca and ^{48}Ca + ^{48}Ca. The whole set of data has been analyzed with the CC model that was used in a similar analysis [14] of the ^{48}Ca + ^{48}Ca fusion measurement of Ref. [11]. More recently, a comprehensive theoretical approach has been applied by Mişicu *et al.* to the systems ^{48}Ca + ^{48}Ca, ^{36}S, and ^{96}Zr [15]. The same dynamical model has been lately employed [16] for the analysis of the preliminary results of the present experiment on ^{40}Ca + ^{40}Ca, shown at a recent conference [17]. The fusion cross sections of ^{40}Ca + ^{40}Ca reported in the present article are the result from the final analysis of the experiment, and differ slightly from the values plotted in Ref. [17], particularly at the lowest energies.

A different and interesting model of low-energy fusion hindrance was developed in Refs. [18,19], where the dynamics of the two touching and overlapping nuclei is calculated at very low energies. Very recently, also the role of quasifission at extreme sub-barrier energies has been emphasized [20].

The fusion measurements on ^{40}Ca + ^{40}Ca are described in the next section, together with the experimental results. CC calculations, using the M3Y + repulsion potential, performed for this system are presented in some detail in Sec. III. Section IV is a full comparison of the evidences coming from the present data and from the recent results obtained for ^{40}Ca + ^{48}Ca and ^{48}Ca + ^{48}Ca. Section V summarizes this work.

II. EXPERIMENT AND RESULTS

The experiment for ^{40}Ca + ^{40}Ca has been performed at the Laboratori Nazionali di Legnaro XTU Tandem Facility, using ^{40}Ca beams in the energy range $E_{\rm lab} = 98$–130 MeV, with intensities up to $\simeq$8–10 pnA. The targets were thin ($\sim$50 μg/cm^2) ^{40}CaF$_2$ evaporations on 15 μg/cm^2 carbon backings. The carbon backings faced the beam. The ^{40}Ca target isotopic enrichment was very high (99.96%). Even with this high enrichment, the lowest measurable cross section resulted to be 10–20 μb, owing to the presence of small quantities of $^{42,43,(44)}$Ca for which the Coulomb barriers in the laboratory system are significantly lower than for ^{40}Ca. Heavier Ca isotopes (mainly ^{48}Ca), although present, were of minor importance because their fusion evaporation products could be discriminated thanks to the mass identification of the detector setup.

The evaporation residues (ERs) were detected near 0° separating out the beam and beamlike particles by an electrostatic filter, already used for several sub-barrier fusion measurements at Laboratori Nazionali di Legnaro (LNL), in its recently upgraded configuration. More details about the filter, as well as a scheme of the detectors downstream, can be found in Ref. [21]. The setup is composed of two microchannel plate detectors for time signals, a ionization chamber for ΔE measurement, and a final 600 mm^2 silicon detector giving the residual energy E_r and the start signal for two independent times of flight (TOFs). Representative examples of raw two-dimensional spectra of E_r-TOF and ΔE-TOF recently obtained for the same setup at sub-barrier energies can be found in Refs. [21,22]. The ER angular distribution was measured at a representative energy ($E_{\rm lab} = 109$ MeV) near the barrier (it was measured at 108 and 120 MeV in the previous experiment [1] and no significant energy dependence was noticed).

The effective solid angle of the complete setup is determined by the final silicon detector and is $\simeq$0.045 msr. Four silicon detectors are used for beam control and normalization between the different runs, placed symmetrically around the beam direction at the same scattering angle $\theta_{\rm lab} = 16°$.

The measured fusion excitation function is shown in Fig. 1, where the reported errors are purely statistical. The absolute cross-section scale is accurate to within ±7%–8% [11,21]. The cross sections agree with the results of a previous experiment [1] (also plotted), apart from the two lowest energy points, where Aljuwair *et al.* [1] obtained larger cross sections. The present data extend further down in energy and a smoother trend is observed below the barrier. At the lowest measured energy ($E_{\rm c.m.} \simeq 48.6$ MeV) no fusion event was observed in a long run of about 8 h. The resulting cross section is quoted as an upper limit corresponding to one fusion event.

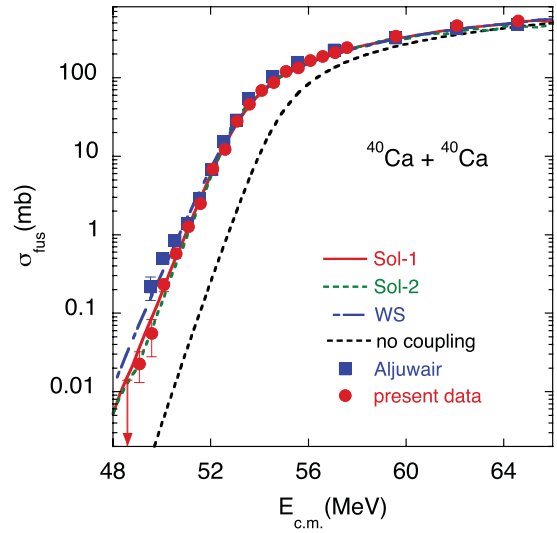

FIG. 1. (Color online) Fusion excitation function of ^{40}Ca + ^{40}Ca measured in the present work and in the previous experiment by Aljuwair *et al.* [1]. CC calculations (lines) are discussed in the text.

The fusion barrier distribution (BD) has been extracted with the usual three-point formula and an energy step of $\simeq$1.5 MeV. It is shown in Fig. 2(a), where BD is normalized to πR_b^2 and R_b is the barrier radius resulting from the Akyüz-Winther potential [23]. The BD derived from the cross sections of Ref. [1] agrees with the present one and can be found in Refs. [6,7]. One main peak dominates the distribution, and a smaller structure may exist a few MeV above, as recently observed for ^{48}Ca + ^{48}Ca [11]. This smaller peak, if real, deserves further investigation [7]. The logarithmic derivative (slope) of the energy-weighted cross section $L(E) = {\rm d}[\ln(E\sigma)]/{\rm d}E$ is reported in Fig. 2(b). It is obtained as the incremental ratio for pairs of points, with energy steps of 1 MeV. One sees a tendency to saturation, or an irregularity of the slope, with decreasing energy just below the main barrier. At the lowest energies the slope seems to increase again, even if the errors are quite large, and the lowest point (having a large error) overlaps with the value L_{CS}. The slope derived from the previous experiment [1] has a well-defined maximum around 52 MeV and decreases at lower energies. The S factor [Fig. 2(c)] appears to reach a maximum vs energy at $E \simeq 49$–50 MeV; however, one would need measurements at lower energies to confirm its existence.

III. COUPLED-CHANNELS ANALYSES

The CC calculations we have performed are similar to those that were made in an analysis [14] of the ^{48}Ca + ^{48}Ca fusion data [11]. The calculations make use of the M3Y + repulsion, double-folding potential which is described in detail in Ref. [24]. The density of ^{40}Ca that is used in calculating the M3Y double-folding potential is parametrized as a symmetrized Fermi function (Eq. (4) of Ref. [14]) with radius R and the diffuseness $a = 0.56$ fm.

The repulsive part of the double-folding interaction is generated by a contact interaction, $v_r\delta(\mathbf{r})$. The density that

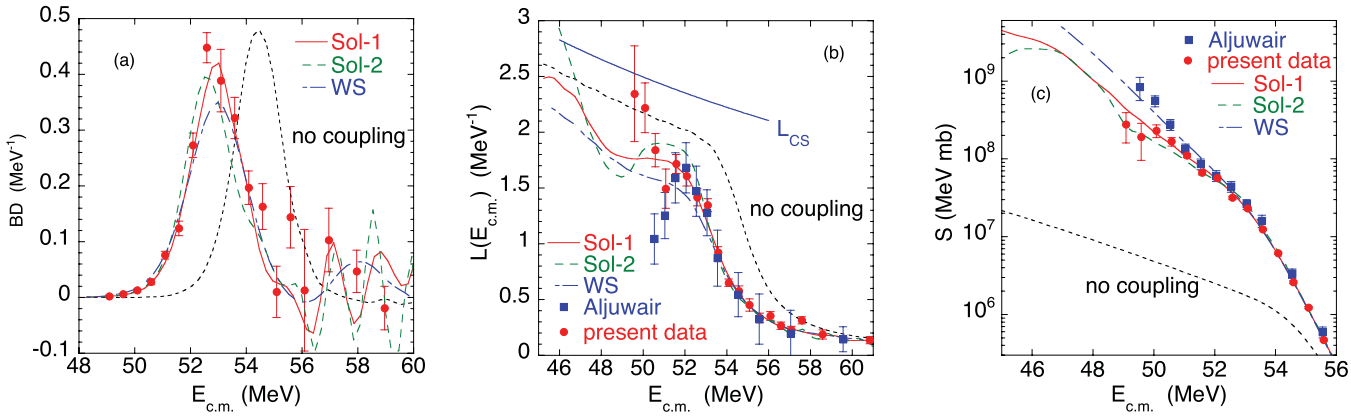

FIG. 2. (Color online) (a) Barrier distribution derived from the present data for ^{40}Ca + ^{40}Ca (solid circles). (b) Logarithmic derivative (slope) $L(E) = \mathrm{d}[\ln(E\sigma)]/\mathrm{d}E$ of the excitation function, obtained using finite steps $\Delta E = 1$ MeV. The line marked L_{CS} is the slope expected for a constant S factor. Here and in the right panel, the data obtained from the previous measurements [1] are plotted as square symbols. (c) The astrophysical S factor. The data are compared to the CC calculations described in the text, which are based on the Woods-Saxon (WS), the M3Y + repulsion (Sol-1, Sol-2) potentials and the associated no-coupling limit using the M3Y + repulsion potential Sol-1.

is used has the same radius as in the M3Y double-folding calculation mentioned above but the diffuseness a_r is adjusted to optimize the fit to the fusion data. The strength of the repulsion v_r is calibrated so that the total M3Y + repulsion potential is consistent with the nuclear incompressibility $K =$ 234 MeV (see Ref. [24] for details). There are two solutions that provide optimum fits to the data when applied in the CC calculations described below. The parameters that generate them are shown in Table I and the resulting entrance channel potentials are shown in Fig. 3. Also shown is the entrance channel potential for a standard Woods-Saxon (WS) potential [23] which has been adjusted to optimize the fit to the data in the CC calculations. The parameters of the WS potential are $R_0 = 8.108$ fm, $a = 0.6525$ fm, and $V_0 = -62.53$ MeV. They produce a Coulomb barrier with the height $V_{\mathrm{CB}} = 54.43$ MeV at the radial separation $R_{\mathrm{CB}} = 9.83$ fm (DR = 0.08 fm). The barrier parameters of the two M3Y + repulsion solutions are shown in Table I.

The nuclear structure input is given in Table II. The Coulomb and nuclear coupling strengths are from an analysis [27] of the elastic and inelastic scattering of ^{16}O on ^{40}Ca. The same reference was also used to determine the structure input for ^{48}Ca in Ref. [14]. The main difference between the two calcium isotopes is that ^{40}Ca is much softer because the 3^- and 5^- states have lower excitation energies and the couplings to theses states are much stronger than in the ^{48}Ca isotope (compare to Table I of Ref. [14]). The full CC calculations that are performed include couplings to the excited states of the projectile and target that are shown in Table II, and to all mutual excitations of the one-phonon states. The two-quadrupole-phonon excitations were also considered (see the lower part of Table II). The energies and adopted $B(E2)$ values of the three members of this two-phonon multiplet have been combined into one effective two-phonon excitation (Eff 2PH), in the same way as in Ref. [14]. Because no experimental information is available for the two-phonon excitations of the 3^- and 5^- states, they have not been considered in the present

TABLE I. Density parameters for ^{40}Ca with the fixed diffuseness $a = 0.56$ fm. The parameter a_r, the radius R, and the rms radius of the best fit solutions to the ^{40}Ca + ^{40}Ca fusion cross sections are shown. The fifth column is the χ^2 per data point obtained from the analysis assuming a 5% systematic error. The two last columns show the barrier height and position. The point-proton radius and rms radius obtained from electron scattering (pp) [25] are also shown.

Solution	a_r (fm)	R (fm)	rms radius (fm)	χ^2/N	V_{CB} (MeV)	R_{CB} (MeV)
Sol-1	0.395	3.43	3.375	1.05	54.46	9.69
Sol-2	0.420	3.47	3.400	1.90	54.45	9.65
pp [25]		3.443	3.383(1)			

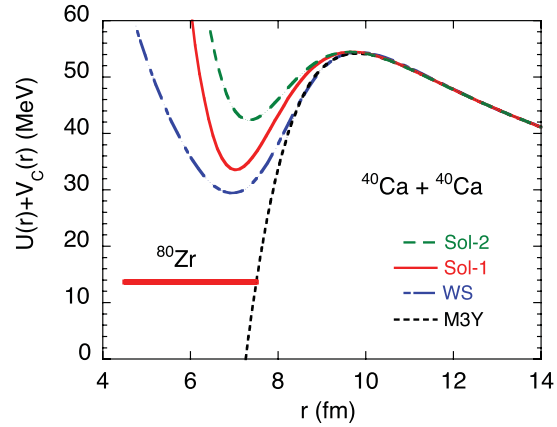

FIG. 3. (Color online) Entrance channel potentials for ^{40}Ca + ^{40}Ca. The ordinate $U(r) + V_{\mathrm{C}}(r)$ is the sum of the nuclear and Coulomb potentials, respectively. The two solutions Sol-1 and Sol-2 are based on the M3Y + repulsion potential. The entrance channel potentials for the Woods-Saxon (WS) and the pure M3Y potentials (without repulsion) are also shown. The horizontal line "^{80}Zr" marks the ground-state energy of the compound nucleus ^{80}Zr at 14.2 MeV.

TABLE II. Nuclear structure input for ^{40}Ca. The $B(E\lambda)$ values are from Ref. [26]. The three transitions shown in the lower part of the Table, have been attributed to the deexcitation of the two-phonon quadrupole triplet, combined in the calculations into one effective state (Eff 2PH, last line, see Ref. [14]).

I^π	E_x (MeV)	$B(E\lambda)$ (W.u.)	$\frac{(\beta R)_C}{\sqrt{4\pi}}$ (fm)	$\frac{(\beta R)_N}{\sqrt{4\pi}}$ (fm)
2_1^+	3.905	2.26(14)	0.138[a]	0.125[a]
3^-	3.737	27(4)	0.465[a]	0.315[a]
5^-	4.491		0.344[a]	0.175[a]
0^+-2_1^+	5.212	17(3)	0.120	
2_2^+-2_1^+	5.249	22(6)	0.163	
4^+-2_1^+	5.279	61(10)	0.363	
Eff 2PH	5.269	41(5)	0.416	0.416

[a]Values from Ref. [27].

calculations. A total of 24 channels were included, and more details can be found in Ref. [14].

Some remarks about the adjustment procedures mentioned above are in order. The data have been always fitted by the full calculations, that is, by CC calculations that include all 24 channels. The adjustments were done consistently, so that when the ion-ion potential is adjusted, the form factors for excitations are changed as well, because the form factors are defined in terms of derivatives of the ion-ion potential. In the case of the WS potential, the radius of the WS well is adjusted, and the derivative form factors are changed accordingly.

The results of the full CC calculations are compared to the present data and to the cross sections of Aljuwair *et al.* [1] in Fig. 1. The calculations are based on the WS and M3Y + repulsion (Sol-1) potentials that optimize the fit to the excitation function. Also shown is the result obtained in the no-coupling limit. The full calculation using the second solution (Sol-2) for the M3Y + repulsion potential is also shown by the (green) dashed curve. This second solution has a larger radius. While the calculation based on the WS potential (blue, dash-dotted line) gives a poor account of the present data, because the cross sections are suppressed compared to this calculation at low energies, it seems to be in fairly good agreement with the results of Aljuwair *et al.* [1] at low energies.

The full calculation (Sol-1, red continuous line) is in good agreement with the present data. However, it slightly overpredicts the two lowest-energy points. The χ^2/N is close to one, according to Table I, when the systematic error is set to 5%. The extracted ^{40}Ca radius of this solution is close to the radius of the point-proton (pp) distribution extracted from electron scattering [25]. The other solution (Sol-2) gives a better fit to the two-three lowest energy points but the overall fit to the data is poorer, with a χ^2/N of the order of 2 (see Table I).

The analysis of the ^{48}Ca + ^{48}Ca fusion data [14] also gave two stable solutions (i.e., they minimize the χ^2/N locally) but in that case it was the solution with the larger radius (Sol-2) that gave the best fit. The solution with the larger radius (Sol-2) has a shallower pocket in the entrance channel potential (see Fig. 3) and it is therefore better suited for explaining data that are strongly hindered at low energies.

The barrier distribution $BD(E)$, the logarithmic derivative of the energy weighted cross sections, $L(E)$, and the S factor for fusion are shown in Fig. 2. The $BD(E)$ is nicely reproduced by the Sol-1 calculation, as well as the S factor apart from the lowest two points which are overpredicted. The calculation based on the WS potential agrees fairly well with the S factors derived from the measured cross sections of Ref. [1].

The experimental slope $L(E)$ is larger than either Sol-1 or Sol-2 calculations below about 50.5 MeV. It appears that both CC calculations predict a steep increase in $L(E)$ but at energies that are lower by $\simeq$3 MeV than observed experimentally. The shape of the Sol-1 curve in Fig. 2(b) is similar to the M3Y + Reid curve in Fig. 5 of Ref. [16]. It is only the way Fig. 5 in Ref. [16] is stretched out that makes it look flatter.

We stress again that the data reported there were taken from a figure in the proceedings of a conference [17]. However, those data were preliminary. Nevertheless, the lowest points (both the present ones and those shown in Fig. 5 of Ref. [16]) overlap with the L_{CS} curve, indicating that a maximum of the S factor is possibly reached. The last sentence of Ref. [16] is not correct. Because the Q value for the formation of the compound nucleus ^{80}Zr is negative ($Q = -14.2$ MeV), the cross section must vanish at 14.2 MeV; hence, it is required that the S factor has a maximum somewhere above that energy (see Eq. (7) of Ref. [12]), which is shown in Fig. 3.

IV. COMPARISON WITH OTHER Ca + Ca SYSTEMS

A. Excitation functions

The measured fusion cross sections of three different calcium isotope combinations are compared in Fig. 4 to the best CC calculations, which, in the case of ^{40}Ca + ^{40}Ca, is based on

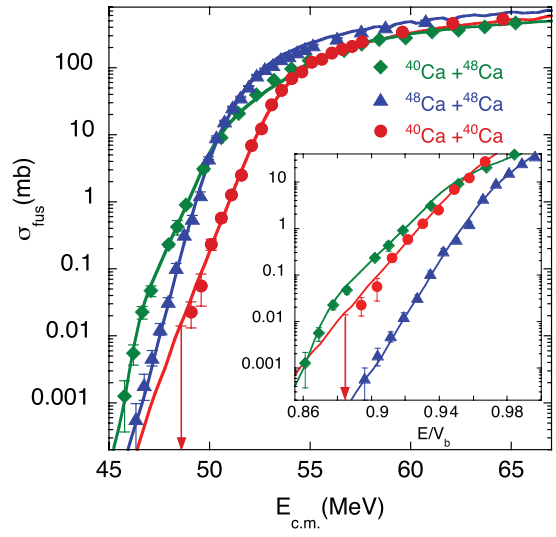

FIG. 4. (Color online) Fusion excitation functions of Ca + Ca systems are compared to the CC calculations that provide the best fits to the data. The inset shows the low-energy cross sections, where the energy scale is normalized to the barrier resulting from the WS potential used in this article [23].

M3Y + repulsion Sol-1 potential. In the case of ^{48}Ca + ^{48}Ca it is based on the Sol-2 potential of Ref. [14]. It is unfortunate that the parameters of the two potentials are so different, in particular the value of a_r which is $a_r = 0.395$ fm for the ^{40}Ca + ^{40}Ca Sol-1 and $a_r = 0.4295$ fm for ^{48}Ca + ^{48}Ca Sol-2. It is therefore difficult to make a prediction for the asymmetric system, ^{40}Ca + ^{48}Ca. Hence, we have readjusted the value of a_r to optimize the fit to the data for this system. The best fit is achieved for $a_r = 0.429$ fm, and that is the value used in the following.

The behavior of the three systems at low energies is clearly observable in the inset of Fig. 4. Its most striking feature is that the cross sections for the asymmetric system ^{40}Ca + ^{48}Ca [13] exceed the data for the larger symmetric system ^{48}Ca + ^{48}Ca [11] at low energies. This can qualitatively be explained by the influence of couplings to transfer channels with positive Q values in the fusion of the asymmetric system, and it parallels the behavior of the three ^{58}Ni + ^{58}Ni, ^{58}Ni + ^{64}Ni, and ^{64}Ni + ^{64}Ni cases, observed in the pioneering work of Beckerman *et al.* [28].

The ^{40}Ca + ^{48}Ca excitation function by Aljuwair *et al.* [1] was reproduced by CC calculations [3] that included couplings to transfer channels with positive Q values. In the present work, the same procedure has been applied to calculate the new ^{40}Ca + ^{48}Ca cross sections by Jiang *et al.* [13]. The result is shown in Fig. 4. The one-nucleon transfer is dominated by one-proton transfer as shown in Ref. [3] and the relevant input is given there. The (two-nucleon) pair transfer has been given an effective Q value of +1 MeV and is described by the form factor, Eq. (4.1) of Ref. [3],

$$V_t = -\sigma_t dU/dr,$$

where $U(r)$ is the WS ion-ion potential discussed earlier. The strength of the best fit to the fusion data is $\sigma_t = 0.39$ fm. We are not able to distinguish the contributions from the $2n$ and $2p$ pair transfer in our analysis. That would require a separate measurement of these reaction channels.

Another interesting feature that can be seen in Fig. 4 is that the cross sections for ^{40}Ca + ^{48}Ca system are suppressed at high energies compared to the data for the two symmetric systems. This is illustrated in the linear plot of Fig. 5 where the excitation functions for the three systems are compared to the best calculations. A weak imaginary potential has here been applied in the CC calculations to reduce the amplitude of the oscillations that occur at high energy. This weak imaginary potential is a WS well with a radius equal to the radial separation of the reacting nuclei at the minimum of the pocket in the entrance channel potential. The strength is −2 MeV, and the diffuseness is 0.2 fm.

The suppression of the data for the asymmetric system is explained nicely by the calculation in which it is caused by the couplings to the transfer channels. Without transfer, the calculation would fall (as naively expected) half-way between the calculations for the two symmetric systems (Fig. 5).

Finally, it is observed in Fig. 4 that the slope of the ^{48}Ca + ^{48}Ca excitation function [11] is much steeper at low energies than the slope of the present ^{40}Ca + ^{40}Ca fusion data. Because

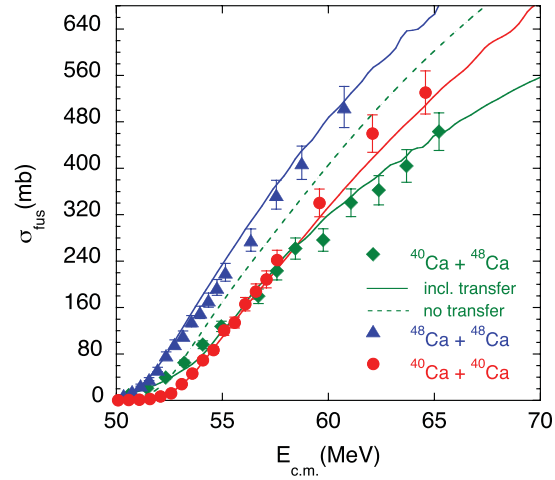

FIG. 5. (Color online) Linear plot of the fusion cross sections for the three systems vs energy. Here the errors include the systematic uncertainty on the absolute cross-section scale (±7%).

the full CC calculations reproduce the two data sets rather well it is possible to investigate what causes this difference in slope. One reason is that the excitation spectrum of ^{40}Ca is much softer, as mentioned earlier than the excitation spectrum of ^{48}Ca. This effect is illustrated in Fig. 6 where the ^{40}Ca + ^{40}Ca fusion cross section has been calculated not only using the (soft) excitation spectrum of ^{40}Ca but also the (stiff) excitation spectrum of ^{48}Ca. It is seen that the softer spectrum produces a larger enhancement and a slightly gentler overall slope of the calculated cross section at energies below but not far away from the Coulomb barrier.

Another reason for the steeper slope of the calculated ^{48}Ca + ^{48}Ca fusion cross section is the ion-ion potential which

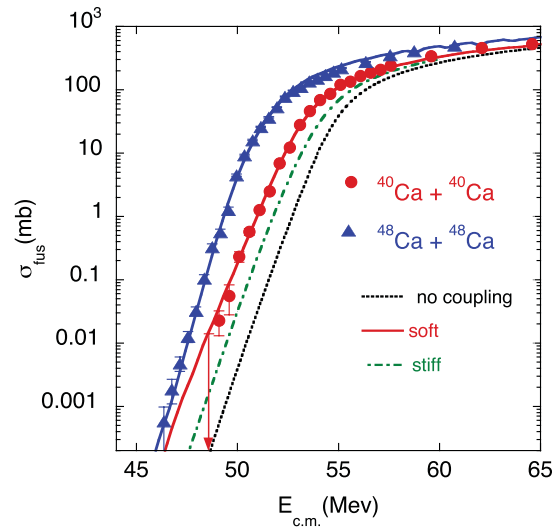

FIG. 6. (Color online) The calculated fusion cross sections for ^{40}Ca + ^{40}Ca obtained in the no-coupling limit (dotted line), using the correct soft ^{40}Ca excitation spectrum (red, full line) and the stiff ^{48}Ca spectrum (green, dash-dotted line), are compared to the data. The measured [11] and calculated [14] fusion cross sections for ^{48}Ca + ^{48}Ca are also shown (blue, continuous line).

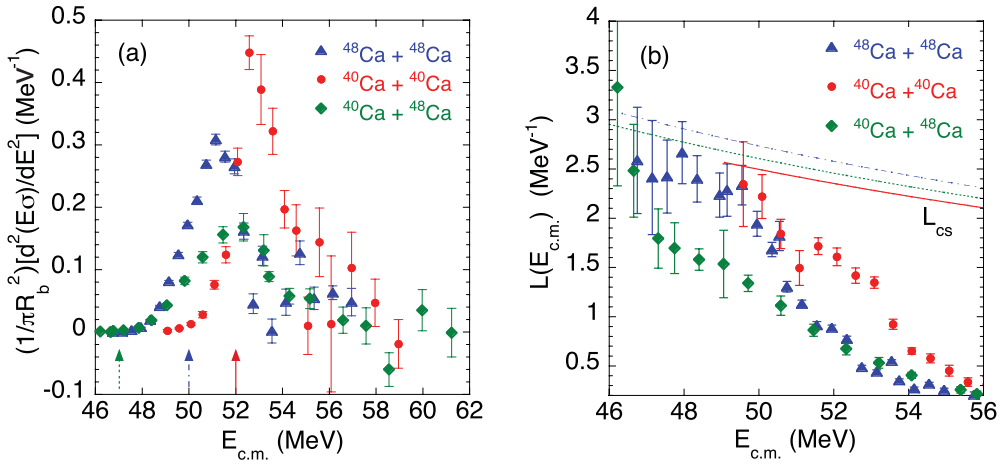

FIG. 7. (Color online) (a) Fusion BDs of ^{40}Ca + ^{40}Ca, ^{40}Ca + ^{48}Ca, and ^{48}Ca + ^{48}Ca. Three arrows are drawn at the energy thresholds of hindrance (see text). (b) Logarithmic derivatives of the three systems. The lines corresponding to L_{CS} are reported for reference. The arrows and the L_{CS} lines are drawn with continuous, dash-dotted, and dotted lines for ^{40}Ca + ^{40}Ca, ^{48}Ca + ^{48}Ca, and ^{40}Ca + ^{48}Ca, respectively.

has a shallow pocket (see Fig. 1 of Ref. [14]), whereas the pocket of the Sol-1 ion-ion potential for ^{40}Ca + ^{40}Ca is deeper so the fusion is less hindered.

The strong sensitivity to structure shown in Figs. 4 and 6 is unambiguous. If we had chosen the Sol-2 potential in all three cases, the interpretation would be straightforward. However, the ^{40}Ca + ^{40}Ca data "prefer" Sol-1, but the fit is not optimal at very low energy. We have no clear explanation of what causes the different behavior of the two systems. For example, higher-lying states than those we have used could be important, or the microscopic form factors we use (expressed in terms of derivatives) could be a poor approximation.

B. Fusion hindrance and nuclear structure

The fusion hindrance phenomenon has been observed in the fusion of many medium heavy systems [9]. This hindrance is usually defined with respect to CC calculations that are based on a standard WS potential. Its onset can often be identified by a sharp increase of the slope $L(E)$, as shown in Figs. 2 and 7(b).

It is noted that, in spite of the large enhancement in the fusion of ^{40}Ca + ^{48}Ca, a hindrance does eventually occur but the onset is pushed down to very low energies, where it sets in rather abruptly below 47 MeV, where $L(E)$ increases rapidly (see Fig. 2(c) of Ref. [13]).

In the case of ^{40}Ca + ^{40}Ca, the hindrance sets in near 52 MeV where the experimental $L(E)$ exceeds the slope of the WS-based CC calculation. This can be seen in Fig. 2(b). The onset of hindrance for ^{48}Ca + ^{48}Ca is near 50 MeV, even though the energy dependence of $L(E)$ is rather flat, according to Fig. 7 of Ref. [14].

In this respect, we compare the fusion BDs for the three systems, extracted from the corresponding measured excitation functions, in Fig. 7(a). When considering the shapes of the BDs, they are essentially symmetric around the main peak for the two symmetric systems. On the contrary, an asymmetric shape shows up for ^{40}Ca + ^{48}Ca, caused by a tail extending toward low energies. This is a further, and independent, clue for the importance of transfer couplings with positive Q values in this system.

In Fig. 7 the vertical arrows mark the hindrance thresholds mentioned above. For ^{40}Ca + ^{40}Ca and ^{48}Ca + ^{48}Ca they are not far below the maximum of the BD, while for ^{40}Ca + ^{48}Ca the hindrance threshold is near the low-energy limit of the tail. It appears that transfer couplings push down the onset of hindrance for this system.

In the energy region far below the barrier for ^{40}Ca + ^{40}Ca (Fig. 4), we can notice that the cross sections start falling off very fast at the two-three lowest energies, analogously to ^{40}Ca + ^{48}Ca. The slope of the excitation functions gives us a clearer insight into these common trends. The logarithmic derivative of the excitation function is very sensitive to small details down there (we are in the μb cross-section range) where nothing is visible from the BDs [29] (see Fig. 7), but where multiphonon excitations of strong modes may still produce barriers with small "weights" [7].

The logarithmic derivatives of the three systems are reported in Fig. 7(b). The two cases with ^{40}Ca show a tendency of the slope to saturate just below the main barrier, and then to increase again for lower energies. On the contrary, a clear saturation shows up and is maintained down to very small energies in ^{48}Ca + ^{48}Ca. This different behavior may possibly be attributable to the strength of the octupole vibration of ^{40}Ca, producing that slope irregularity, as suggested recently [17], not far below the main barrier.

It has been suggested [13] that the neutron excess influences the behavior of cross sections at very low energies, that is, in nearby systems the threshold energy for hindrance and the energy location of the S factor maximum are lower for the cases with a larger N-Z. The present Ca + Ca systematics, however, make it possible to observe that the concurring influence of the softer excitation spectrum of ^{40}Ca and, on top of that, of couplings to transfer channels with positive Q values in ^{40}Ca + ^{48}Ca, make it difficult to recognize the effect of the neutron excess.

V. SUMMARY

In this article we have reported the results of a new measurement of the fusion excitation function for the system ^{40}Ca + ^{40}Ca from well below to well above the Coulomb barrier. The present data greatly extend the results of a previous experiment [1], down to $\sigma \simeq 20\ \mu$b. At the lowest energies the logarithmic derivative of the excitation function increases rather fast and almost reaches the L_{CS} value expected for a constant astrophysical S factor. As a consequence, there is a tendency for the S factor to develop a maximum as a function of the energy. Further data at still lower energies would be strongly needed. The fusion BD of ^{40}Ca + ^{40}Ca has one main peak with, possibly, a smaller structure $\simeq$4 MeV higher in energy.

Coupled-channels calculations have been performed using the M3Y + repulsion, double-folding potential, in analogy to the recent analysis of the ^{48}Ca + ^{48}Ca system [14]. This has allowed a good description of the excitation function, with an ion-ion potential that is not so shallow as in the case of ^{48}Ca + ^{48}Ca, although the two lowest-energy points are slightly overestimated (as in Ref. [16]). The BD of ^{40}Ca + ^{40}Ca is nicely fitted by the CC results. A sharp increase in the logarithmic derivative of the excitation function below the barrier is predicted at an energy $\simeq$3 MeV lower than observed experimentally. The reason why it is so deserves further theoretical investigation, as well as the difference between this system and ^{48}Ca + ^{48}Ca.

Specific calculations for ^{40}Ca + ^{48}Ca show that nucleon-transfer channels with positive Q values enhance the sub-barrier fusion cross sections, as observed in a comparison with the two symmetric systems. Such transfer couplings are probably responsible for the low-energy tail of the BD observed only for ^{40}Ca + ^{48}Ca. When comparing with the previous results of Refs. [4,13], the CC calculations we have presented here provide a fairly consistent description of the data for all three systems, although there are some uncertainties. For example, measurements of the one- and two-nucleon transfer would be welcome, so that the strength of the pair transfer we have used can be tested or calibrated.

The experiments described here are very challenging. Comparing with earlier studies, the present new results on ^{40}Ca + ^{40}Ca, together with our recent measurements on ^{40,48}Ca + ^{48}Ca [11,13] have allowed a much deeper insight into the fusion dynamics of these Ca + Ca systems at energies far below the Coulomb barrier. The behavior of ^{40}Ca + ^{40}Ca differs significantly from both ^{48}Ca + ^{48}Ca and ^{40}Ca + ^{48}Ca cases.

We stress once more that further measurements at still lower energies for ^{40}Ca + ^{40}Ca would be very useful to fully establish the inadequacy of a WS potential to fit its excitation function down to the sub-μb range (as reported in Ref. [14] for ^{48}Ca + ^{48}Ca), and of course to clear up the existence of a maximum of the S factor at $\simeq$49–50 MeV. Indeed, a maximum of S develops if the hindrance is strong enough to bring the slope up to the L_{CS} value.

Different slopes of the excitation functions show up for ^{40}Ca + ^{40}Ca and ^{48}Ca + ^{48}Ca below the barrier, at least partly as a consequence of the different strength of the octupole vibration in ^{48}Ca and ^{40}Ca. Fusion hindrance is observed for all three systems with differing features, and it appears that its onset is pushed down to rather low energies for the asymmetric case, possibly owing to transfer couplings. It is very interesting that nuclear structure effects can be revealed at energies so far below the Coulomb barrier.

ACKNOWLEDGMENTS

We are indebted to N. Rowley for several discussions on the importance of octupole states in calcium isotopes. Grateful thanks are due to the XTU Tandem staff for their professional work, to M. Loriggiola for excellent target preparation, and to F.Scarpa, D. Martini for producing the high-quality calcium beams in the ion source. C.L.J., H.E., and K.E.R. are supported by the U.S. Department of Energy, Office of Nuclear Physics, Contract No. DE-AC02-06CH11357. X.D.T. is supported by the NSF under Grants No. PHY-0758100 and No. PHY-0822648 and the University of Notre Dame.

[1] H. A. Aljuwair, R. J. Ledoux, M. Beckerman, S. B. Gazes, J. Wiggins, E. R. Cosman, R. R. Betts, S. Saini, and O. Hansen, Phys. Rev. C **30**, 1223 (1984); H. A. Aljuwair, Ph.D. thesis, Massachusetts Institute of Technology, 1983 (unpublished).
[2] M. Beckerman, Rep. Prog. Phys. **51**, 1047 (1988).
[3] H. Esbensen, S. H. Fricke, and S. Landowne, Phys. Rev. C **40**, 2046 (1989).
[4] M. Trotta, A. M. Stefanini, L. Corradi, A. Gadea, F. Scarlassara, S. Beghini, and G. Montagnoli, Phys. Rev. C **65**, 011601 (2001).
[5] N. Rowley, G. R. Satchler, and P. H. Stelson, Phys. Lett. B **254**, 25 (1991).
[6] M. Dasgupta, D. J. Hinde, N. Rowley, and A. M. Stefanini, Annu. Rev. Nucl. Part. Sci. **48**, 401 (1998).
[7] N. Rowley and K. Hagino, Nucl. Phys. A **834**, 110c (2010).
[8] C. L. Jiang, H. Esbensen, K. E. Rehm, B. B. Back, R. V. F. Janssens, J. A. Caggiano, P. Collon, J. Greene, A. M. Heinz, D. J. Henderson, I. Nishinaka, T. O. Pennington, and D. Seweryniak, Phys. Rev. Lett. **89**, 052701 (2002).
[9] C. L. Jiang, B. B. Back, H. Esbensen, R. V. F. Janssens, and K. E. Rehm, Phys. Rev. C **73**, 014613 (2006).
[10] M. Dasgupta, D. J. Hinde, A. Diaz-Torres, B. Bouriquet, C. I. Low, G. J. Milburn, and J. O. Newton, Phys. Rev. Lett. **99**, 192701 (2007).
[11] A. M. Stefanini, G. Montagnoli, R. Silvestri, L. Corradi, S. Courtin, E. Fioretto, B. Guiot, F. Haas, D. Lebhertz, P. Mason, F. Scarlassara, and S. Szilner, Phys. Lett. B **679**, 95 (2009).
[12] C. L. Jiang, H. Esbensen, B. B. Back, R. V. F. Janssens, and K. E. Rehm, Phys. Rev. C **69**, 014604 (2004).
[13] C. L. Jiang, A. M. Stefanini, H. Esbensen, K. E. Rehm, L. Corradi, E. Fioretto, P. Mason, G. Montagnoli, F. Scarlassara, R. Silvestri, P. P. Singh, S. Szilner, X. D. Tang, and C. A. Ur, Phys. Rev. C **82**, 041601(R) (2010).
[14] H. Esbensen, C. L. Jiang, and A. M. Stefanini, Phys. Rev. C **82**, 054621 (2010).
[15] S. Mişicu and F. Carstoiu, Phys. Rev. C **83**, 054622 (2011).
[16] S. Mişicu and F. Carstoiu, Phys. Rev. C **84**, 051601(R) (2011).

[17] G. Montagnoli and A. M. Stefanini, *Proceedings of the International Conference on FUSION11, Saint-Malo, France, 2–6 May 2011*, EPJ Web of Conferences, edited by Ch. Schmitt, A. Navin, M. Rejmund, D. Lacroix, and H. Goutte (2011), Vol. 17, p. 05001.
[18] T. Ichikawa, K. Hagino, and A. Iwamoto, Phys. Rev. C **75**, 064612 (2007).
[19] T. Ichikawa, K. Hagino, and A. Iwamoto, Phys. Rev. Lett. **103**, 202701 (2009).
[20] V. V. Sargsyan, G. G. Adamian, N. V. Antonenko, W. Scheid, and H. Q. Zhang, Phys. Rev. C **84**, 064614 (2011).
[21] A. M. Stefanini, G. Montagnoli, L. Corradi, S. Courtin, E. Fioretto, A. Goasduff, F. Haas, P. Mason, R. Silvestri, P. P. Singh, F. Scarlassara, and S. Szilner, Phys. Rev. C **82**, 014614 (2010).
[22] A. M. Stefanini, G. Montagnoli, R. Silvestri, S. Beghini, L. Corradi, S. Courtin, E. Fioretto, B. Guiot, F. Haas, D. Lebhertz, N. Mărginean, P. Mason, F. Scarlassara, R. N. Sagaidak, and S. Szilner, Phys. Rev. C **78**, 044607 (2008).
[23] Ö. Akyüz and Å.Winther, in *Nuclear Structure and Heavy-Ion Physics*, Proceedings of the International School of Physics "Enrico Fermi," Course LXXVII, Varenna, edited by R. A. Broglia and R. A. Ricci (North Holland, Amsterdam, 1981).
[24] S. Mişicu and H. Esbensen, Phys. Rev. C **75**, 034606 (2007).
[25] I. Angeli, At. Data Nucl. Data Tables **87**, 185 (2004).
[26] Evaluated Nuclear Structure Data Files, National Nuclear Data Center, Brookhaven National Laboratory [http://www.nndc.bnl.gov/].
[27] H. Esbensen and F. Videbaek, Phys. Rev. C **40**, 126 (1989).
[28] M. Beckerman, M. Salomaa, A. Sperduto, H. Enge, J. Ball, A. DiRienzo, S. Gazes, Yan Chen, J. D. Molitoris, and M. Nai-feng, Phys. Rev. Lett. **45**, 1472 (1980).
[29] C. Dasso, J. Phys. G **23**, 1203 (1997).